Magnetic Resonance Imaging to Measure Concentration Profiles of Solutes Diffusing in Stagnant Beds of Cellulosic Fibers

E. J. Tozzi
Dept. of Chemical Engineering and Material Science, University of California, Davis, CA 95616

D. M. Lavenson
Dept. of Chemical Engineering and Material Science, University of California, Davis, CA 95616

M. J. McCarthy
Dept. of Biological and Agricultural Engineering, University of California, Davis, CA 95616

R. L. Powell
Dept. of Chemical Engineering and Material Science, University of California, Davis, CA 95616

DOI 10.1002/aic.12578
Published online April 1, 2011 in Wiley Online Library (wileyonlinelibrary.com).

The evolution of the concentration profiles of an adsorbing solute diffusing in a stagnant bed of cellulosic fibers is measured using magnetic resonance imaging. Effective diffusivities are calculated by matching concentration profiles with a numerical model of one-dimensional Fickian diffusion. The measured values of the effective diffusion coefficients are interpreted using a model that accounts for the porosity, tortuosity, and adsorption equilibrium constant. The effective diffusivities in fiber beds are significantly lower than the bulk diffusivity of the solute and highly dependent on fiber type. The diffusivity is lower for the fiber type that exhibited stronger adsorption properties. The influence of concentration, adsorption, and other fiber characteristics on diffusion rates and rates of reaction is discussed. © 2011 American Institute of Chemical Engineers *AIChE J,* 58: 59–68, 2012

Keywords: magnetic resonance imaging, diffusion coefficient, adsorption, cellulosic fibers, biomass

Introduction

Unit operations involving fibrous suspensions are prevalent in pulp processing, paper making, food processing and in the rapidly developing area of conversion of biomass into fuels and chemicals.[1,2] Optimizing these processes poses significant challenges due to the interactions between fibers, which lead to a complex microstructure. This microstructure deforms under applied stresses resulting in nonlinear rheological properties that are difficult to characterize. Other transport properties are also strongly influenced by the microstructure and the properties of the fibers themselves. For example, diffusion is a key mechanism of mass transport in operations that involve mixing and chemical reactions of solutes in suspensions of cellulosic fibers. It is expected that the diffusion coefficient will be strongly influenced by the fiber microstructure and the complex interactions that occur between the diffusing species and individual fibers.

The economics of biomass processing require the use of high concentrations of fibers, which results in operation at high viscosity.[3–6] Rates of enzymatic liquefaction of highly

Correspondence concerning this article should be addressed to E. J. Tozzi at ejtozzi@ucdavis.edu.

viscous suspensions have been shown to be a strong function of mixing quality.[7] Suspensions must be well mixed to ensure uniform enzyme distribution, uniform pH and temperature, and to avoid localized hydrolysis product build-up which would reduce reaction rates.[8] Mixing concentrated fiber suspensions is a challenge due to the complex microstructure, which leads to high viscosities and yield stresses. An efficient way to mix highly viscous materials containing an initially heterogeneous distribution of solute is to deform it into a stack of layers by repeated stretching and folding. As the layers become thinner, diffusion becomes the dominant homogenizing mechanism.[9,10] The amount of energy necessary to economically mix the material to a specified degree of homogeneity in a reasonable time is a function of diffusion rates. More specifically, higher diffusion rates result in more rapid homogenization and require less mechanical energy. The diffusion process must also be quantitatively understood to model the kinetics of biomass pretreatment for biofuels production.[11]

Various factors influence diffusion in fibrous materials. At a microscopic or individual fiber level, diffusion of chemicals through wood and cellulosic particles is highly anisotropic due to the complex capillary structure of fibers.[12,13] The type of cellulosic material has a great influence on diffusion. Kim and Lee[14] measured uptake rates of sulfuric acid on particles of corn stover, sugar cane bagasse, rice straw and yellow poplar. They ground the materials using a cutting mill and sieved to mesh sizes of 14–20 and 20–24. They reported that intra-particle diffusivities of sulfuric acid in agricultural residues were much larger than in ground yellow poplar.

Although a fiber suspension is microscopically heterogeneous, it can be macroscopically modeled as a porous medium with an effective diffusivity D_{eff}. A scalar effective diffusivity is used for beds of randomly oriented fibers. There are few reports on effective diffusivities in cellulosic fiber beds. Paterson and Kerekes[15] measured diffusion and reaction of chlorine on unbleached Kraft pulps at 2.1% w/w (''low consistency'') and 12.8% w/w (''medium consistency''). They followed the chlorine front in the suspension as a function of time. This front advanced very slowly, $\sim$2 mm/h, for the 12.8% w/w pulp and 5 mm/h for the 2.1% w/w pulp. Since chlorination is quite rapid, diffusion is the rate limiting step in bleaching fibers, especially at medium consistency. Hence, diffusive transport must be augmented by mixing to achieve industrially rapid mass transfer that allows the reaction process to occur homogeneously and quickly. Wong and Reeve[16] measured diffusivity of potassium chloride in beds of various fiber types, including nylon, wood pulp, cut wood pulp, and ''super absorbent'' cellulosic fibers. They reported that the effective diffusivity in the fiber bed decreased linearly with volumetric fiber concentration, where the volume of water entrapped in individual fibers is included in the fiber volume.

All of the aforementioned experimental studies assume that the diffusion process is governed by Fick's second law. In one-dimension, this is represented by

$$\frac{\partial C}{\partial t} = D_{\text{eff}} \frac{\partial^2 C}{\partial z^2}, \tag{1}$$

where C is concentration, t is time, z is the spatial coordinate along the direction of diffusion, and D_{eff} is the constant effective diffusion coefficient. For the systems studied here, this effective diffusivity lumps together classical diffusion effects due to Brownian motion, adsorption effects due to fiber/solute interactions and a hindered diffusion effect due to the fluid volume excluded by the presence of the particles and the consequent geometrical constraints imposed upon a solute molecule.

The influence of the geometrical features of a porous medium on diffusive transport without adsorption is usually described by[17]

$$D_{\text{eff}}^{\text{Porous}} = \frac{\varepsilon}{\tau} D_0, \tag{2}$$

where D_0 is the bulk diffusivity, ε is the void fraction (ratio of volume of continuous phase and total volume), and τ is the tortuosity factor, which depends on the shape and arrangement of the particles.[18] The void fraction, $\varepsilon = 1-\phi$, decreases linearly as fiber volume fraction, ϕ, is increased. Equation 2 shows that diffusion is more strongly impeded for suspensions with low void fraction (high solids fraction) and high tortuosity.

Cellulosic fibers are not inert and may interact with the solutes being transported through the fibrous bed, which may reversibly adsorb to fibers. In the enzymatic conversion of biomass to sugars, enzymes, coadjuvant proteins and surfactants, all can adsorb to the substrates.[19–24] Divalent cations are also adsorbed onto cellulosic surfaces, which can act as ion exchangers.[25–27] The effect of adsorption equilibrium on the apparent diffusion coefficient in a homogeneous medium is described by[28,29]

$$D_{\text{eff}}^{\text{Adsorbing}} = \frac{D_0}{1+R}, \tag{3}$$

where R is the slope of a linear adsorption isotherm that describes the adsorption process. In this model it is assumed that the solute concentration is small and a linear adsorption equilibrium applies,

$$C_{\text{adsorbed}} = R\, C_{\text{mobile}}, \tag{4}$$

where C_{adsorbed} is the concentration of the adsorbed species, and C_{mobile} is its concentration in the phase through which the solute is mobile. Both concentrations are defined per unit volume of suspension. From Eq. 3, strong adsorption, $R \gg 1$, has the effect of reducing the apparent diffusivity. To account for the porous geometry and adsorption, the parameters from Eqs. 2 and 4 are combined to obtain[30]

$$D_{\text{eff}} = \frac{\varepsilon D_0}{\tau(1+R)}. \tag{5}$$

This diffusivity model also applies for nonlinear adsorption isotherms (i.e., Langmuir) with an initial linear region, as long as the solute concentrations remain within the linear (low concentration) region. An extension of the model is required when particles have significant internal porosity. If the dimensions of the pores are comparable with the size of the diffusing molecule, the apparent diffusion coefficient is

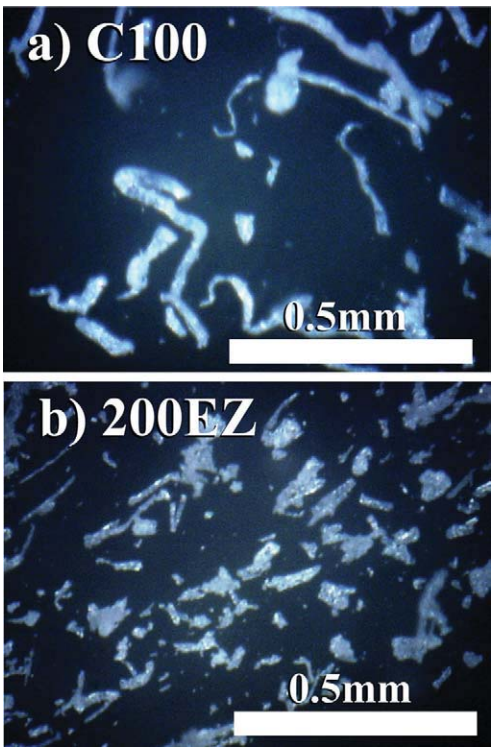

Figure 1. Micrographs of cellullosic fibers used.

[Color figure can be viewed in the online issue, which is available at wileyonlinelibrary.com.]

lowered due to additional interactions between the solute and the pore walls. Reviews of various models for hindered diffusion can be found in Deen[31] and Phillips et al.[32] Other factors that are known to influence diffusion in porous media and are not addressed in this work include: (a) effects of electrical charge, which can alter diffusion rates due to changes in attractive-repulsive interactions between solute and fiber surface; (b) particle alignment, which requires the use of a diffusion tensor rather than a scalar to describe diffusivity in an anisotropic medium.

Modeling transport of solutes in biomass requires the determination of material properties, especially diffusivity, in complex systems that are usually heterogeneous and opaque. Making these measurements is challenging in cellulose suspensions at concentrations typical of pulp and paper processing but even more so for biomass processes that operate at much higher concentrations. Specifically, it is necessary to determine spatially resolved concentration fields in concentrated suspensions for a solute that diffuses and adsorbs reversibly. Such measurements can be made using magnetic resonance (MR) imaging.[33] Here we use this technique with a water-cellulosic fiber matrix to measure concentration profiles of $MnCl_2$ as a function of time. Two types of cellulosic fibers having different sizes and adsorption equilibrium constants were used. The concentration profiles as a function of time were compared with a numerical model based on one-dimensional Fickian diffusion. The measured values of effective diffusion coefficients are interpreted using an equation that accounts for the porosity, tortuosity, and adsorption equilibrium constant, Eq. 5.

Materials and Methods

Two grades of commercial delignified cellulosic fibers (Solka-Floc, International Fiber Corporation, Tonawanda, NY) were used: C100 and 200EZ. Micrographs of the two fibers, Figure 1, clearly show that the C100 grade consists of longer particles than the 200EZ grade. Fiber sizes were measured with an "L&W FiberTester" (Lorenz and Wettre, Kista, Sweden) and are given in Table 1. Here L_{LW} represents the length-weighted average length defined as[34]

$$L_{LW} = \frac{\sum (l_i n_i) l_i}{\sum n_i l_i}, \tag{6}$$

where n_i is the number of fibers belonging to the length class l_i, and the summations are over the number of particles in the sample. The length-weighted average width is similarly defined, W_{LW}. The number-weighted average length is

$$L_{NW} = \frac{\sum (l_i n_i)}{\sum n_i}. \tag{7}$$

The moisture content of the fibers was measured using a moisture analyzer (Mettler-Toledo model HR83).

The diffusing solute used was manganese chloride ($MnCl_2$) (Fischer Scientific, Pittsburgh, PA). This solute was chosen due to its strong paramagnetic properties that facilitate the detection of micromolar concentration levels with nuclear MR imaging.

A 1 Tesla permanent magnet based imaging spectrometer (Aspect Magnet Technologies, Hevel Modi'in Industrial Area, Israel), with 0.3 T/m peak gradient strength was used for imaging. Images were obtained using a Spin Echo sequence (TE=10 ms, TR=300 ms). The radio frequency coil is a solenoid with four turns, encasing a cylindrical volume 60 mm in diameter and 60 mm long. The system arrangement is illustrated in Figure 2 with an example image.

Calibration

Calibration curves for the concentration of $MnCl_2$ were obtained by measuring the absolute MR signal, S, for various concentrations of $MnCl_2$ and comparing it to the absolute MR signal for a pure water reference in the same image, S_w. The MR signal is a function of $MnCl_2$ concentration since the proton relaxation times (spin-spin relaxation time and spin-lattice relaxation time) are functions of $MnCl_2$ concentration. The calibration curve was constructed by taking the ratio of S to S_w and plotting the value vs. $MnCl_2$ concentration. Such curves were obtained

Table 1. Characteristics of Fibers Used

Variable	Fiber Type	
	C100	200EZ
Moisture content (%)	5.75	6.80
L_{LW} (μm)	349	207
L_{NW} (μm)	273	183
W_{LW} (μm)	31.7	26.4

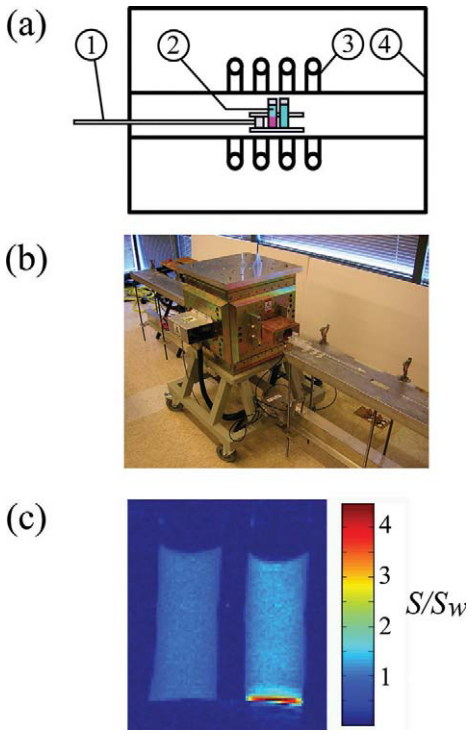

Figure 2. (a) Parts of the imaging system (not to scale): (1) Sample holder; (2)Vials with samples; (3) RF coil; (4) Magnet enclosure. (b) Exterior view of the system. (c) Example of images obtained. A vial with water (left), and a vial a $MnCl_2$ solution and a small amount of fibers at the bottom (right).

[Color figure can be viewed in the online issue, which is available at wileyonlinelibrary.com.]

for $MnCl_2$ in water and $MnCl_2$ in suspensions of each fiber and are shown in Figure 3. These data were fit to the function

$$S/S_w = k_1\left(1 - \exp^{-k_2 \cdot C}\right) + k_3, \tag{8}$$

Where C is the concentration of $MnCl_2$. Parameters k_1, k_2 and k_3 were obtained by nonlinear fit for $MnCl_2$ in fiber suspensions. For $MnCl_2$ in water, only parameters k_1 and k_2 were computed by nonlinear fit, because when $C = 0$, the signal ratio is $S/S_w = 1$, and the third parameter is $k_3 = 1$. Samples for calibration and diffusion experiments had a fiber concentration corresponding to the packing fraction obtained by gravity settling, which was approximately 8.8% volume for C100 and 11.9% volume for 200EZ.

Adsorption

To obtain adsorption equilibrium constants a small mass of fibers, m, was added to a cuvette containing a homogeneous water-tracer mixture of known concentration $C_0' = 95$ mol/m^3. We use the "prime" notation to indicate moles of solute per unit of liquid volume, as opposed to moles per unit of suspension volume. After equilibration the concentration in the supernatant C'_{mobile} was measured using Eq. 8. A plot of C'_{mobile} as a function of mass m of fibers added is shown in Figure 4. For both fibers, as the mass of cellulose increases, C_{mobile}' decreases. This results from the increased number of fibers that can adsorb the $MnCl_2$ and thereby reduce the amount of solute present in the liquid phase. The effect is stronger for the C100 fibers than for the 200EZ. It must be noted that if the fibers had similar surface properties, it is expected from a surface area standpoint alone that the shorter fibers (200EZ) would have larger surface area, and therefore more adsorbing sites. The measurements indicate that the C100 fibers have more adsorbing sites per unit area than 200EZ fibers. Adsorption properties of cellulosic fibers can vary greatly depending on their source and chemical treatments used to prepare them.[35]

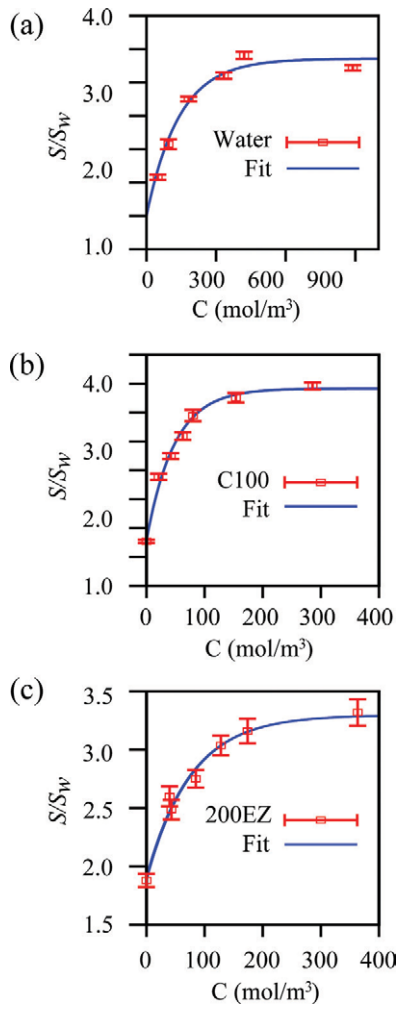

Figure 3. Signal calibration curves for $MnCl_2$ in water (a) and the two types of cellulose fibers; c100 (b), 200EZ(c). The normalized MR signal S/S_w is plotted as a function of the concentration of $MnCl_2$ (mol/m^3).

[Color figure can be viewed in the online issue, which is available at wileyonlinelibrary.com.]

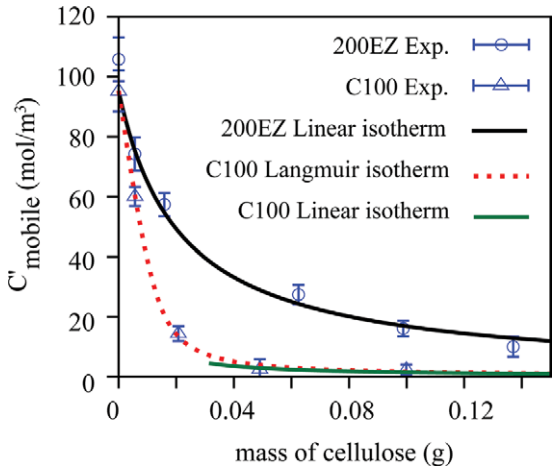

Figure 4. Concentration of $MnCl_2$ remaining in the supernatant as a function of added mass of fibers into a vial.

[Color figure can be viewed in the online issue, which is available at wileyonlinelibrary.com.]

The moles of solute adsorbed per unit mass of fibers M_{adsorbed} are

$$M_{\text{adsorbed}} = \frac{(C'_0 - C'_{\text{mobile}})V}{m}, \tag{9}$$

where V is the volume of the liquid phase and m is the mass of fibers. A plot of M_{adsorbed} as a function of concentration in the mobile phase C'_{mobile} is shown in Figure 5. The adsorption isotherm for the C100 fibers shows saturation behavior at large concentrations. This can be fit to a Langmuir equation

$$M_{\text{adsorbed}} = \frac{k\Gamma^{\infty}C'_{\text{mobile}}}{1 + kC'_{\text{mobile}}}, \tag{10}$$

which at low concentrations has the limiting slope $K_{\text{ads}}^{\text{C100}} = k\Gamma^{\infty} = 2.71$ m^3/kg. Saturation was not observed for 200EZ fibers for the concentration range studied, and therefore a linear fit was used to compute the adsorption constant of the 200EZ fibers $K_{\text{ads}}^{\text{200EZ}} = 0.197$ m^3/kg.

The dimensionless adsorption constant R for each fiber is calculated from K_{ads}

$$R = \frac{C_{\text{adsorbed}}}{C_{\text{mobile}}} = \frac{M_{\text{adsorbed}}\, m}{V_{\text{total}} C_{\text{mobile}}} = \frac{K_{\text{ads}} m}{V}, \tag{11}$$

taking into account that $C'_{\text{mobile}} \cdot V = C_{\text{mobile}} \cdot V_{\text{total}}$, where V_{total} is the volume of suspension that contains a volume of liquid V.

Diffusion

To measure diffusion coefficients we prepared beds of fibers with two distinct concentration layers; the bottom layer with a known concentration of $MnCl_2$ and the top layer without any $MnCl_2$. This initial concentration profile with a large gradient was designed to cause a substantial diffusive flux from the region rich in $MnCl_2$ to the region of low concentration. Concentration profiles were measured at different times using MR imaging. Data are presented as solute concentration as a function of position at different times. From the changes over time of the concentration profiles we computed effective diffusivities as described below.

Calculation of Experimental Effective Diffusivities

Effective diffusivities were computed following Olson et al.,[33] by matching the experimental concentration profiles with profiles calculated by numerically solving the one-dimensional diffusion equation. The numerical solution is found using the Crank-Nicolson finite-difference method.[29] The experimentally measured concentration profile $C_0(z)$ is used as the initial condition at $t = 0$. The boundary conditions used are of the von Neumann type,

$$\frac{\partial C}{\partial z} = 0 \quad \text{at } z = 0 \text{ and } z = L, \tag{12}$$

representing no-flow of solute through the upper and lower boundary.

Numerical concentration profiles are computed at different time steps, following the procedure described by Crank.[29] By finding at which time steps the experimental and numerical concentration profiles are matched in a sum-of-squares sense, we find an experimental effective diffusivity $D_{\text{eff}}^{\text{Exp}}$ as

$$D_{\text{eff}}^{\text{Exp}}(t) = \frac{j\Delta\hat{t}L^2}{t}, \tag{13}$$

where t is the time at which the concentration profile was measured, L is the bed length, $\Delta\hat{t}$ is the size of each dimensionless time step, and j is the number of dimensionless time steps required for matching between the experimental and numerical concentration profiles.

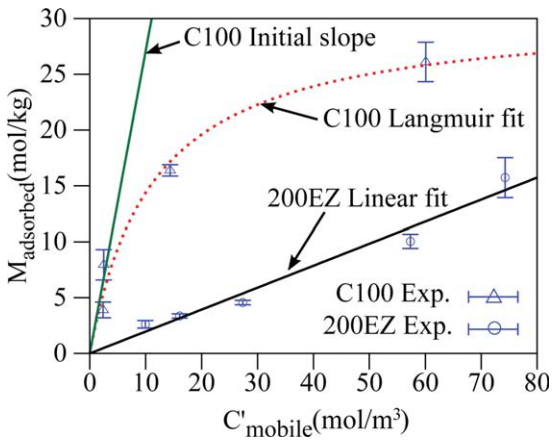

Figure 5. Adsorption isotherms for $MnCl_2$ on two types of cellulose fibers. Adsorbed $MnCl_2$ (mol/kg cellulose) is plotted as a function of the mobile Mn concentration (mol/m^3).

[Color figure can be viewed in the online issue, which is available at wileyonlinelibrary.com.]

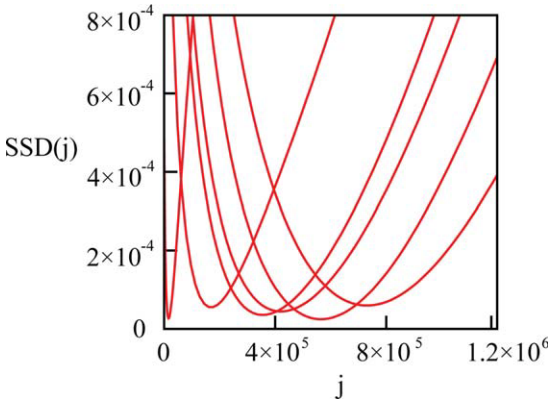

Figure 6. Minima of *SSD(j)* are used to calculate $D_{eff}^{Exp}(t)$.

[Color figure can be viewed in the online issue, which is available at wileyonlinelibrary.com.]

The matching to compute the effective diffusivity is achieved by finding the number of dimensionless time steps j at which the function

$$SSD(j) = \sum_{z=0}^{z=L} \left(\frac{C_{Exp}(z)}{\langle C_{Exp} \rangle} - \frac{C_{Num}(z)}{\langle C_{Num} \rangle} \right)^2 \tag{14}$$

is minimized, where $SSD(j)$ is the sum of the squared differences between the experimental concentrations $C_{Exp}(z)$ profile and the numerical concentrations $C_{Num}.(z)$, made dimensionless using spatially averaged concentrations $\langle C_{Exp} \rangle$ and $\langle C_{Num} \rangle$ respectively. Plots of $SSD(j)$ curves corresponding to $C_{Exp}(z)$ measured at different times for C100 fibers are shown in Figure 6.

The diffusivities thus calculated are plotted in Figure 9. The best estimate of D_{eff}^{Exp} is obtained as the mean value of the $D_{eff}^{Exp}(t)$ computed for each fiber type. The standard deviation of the $D_{eff}^{Exp}(t)$ values is used as a measure of uncertainty.

Results and Discussion

Concentration profiles of $MnCl_2$ in beds of both types of fibers are plotted in Figures 7 and 8. The spatially averaged concentrations $\langle C \rangle$, are 29 mol/m^3 and 36 mol/m^3 for C100 and 200EZ fibers, respectively. At the concentrations used, $C_{mobile}' = C/(1 + R)$ is within the linear region of the adsorption isotherms for both fibers. The length of the fiber beds, L, is 16.7×10^{-3} m and 11.7×10^{-3} m for C100 and 200EZ fibers, respectively. Data obtained at different times are shown along with curves calculated using the numerical method described previously. At a particular time, the solution to the diffusion equation was found using the initial condition obtained from an experimental measurement, shown in the top graph in Figures 7 and 8.

Values of D_{eff}^{Exp} were obtained at different times for each type of fiber by matching the numerical and experimental concentration profiles (Figure 9). The experimentally measured effective diffusivities remained constant within experimental precision, which indicates that the evolution of the concentration is consistent with a Fickian diffusion model with a constant D_{eff}^{Exp}. The values of the effective diffusivities for the C100 and 200EZ fiber suspensions are $(4.39 \pm 0.5) \times 10^{-12}$ m^2/s and $(4.37 \pm 0.4) \times 10^{-11}$ m^2/s, respectively, whereas the diffusion coefficient for $MnCl_2$ in water at 25°C is $D_0 = 1.26 \times 10^{-9}$ m^2/s, from Refs. 17,33,36. The values reflect that diffusion of $MnCl_2$ is much slower in the presence of fibers.

To interpret the results, we compare the measured values D_{eff}^{Exp} with predictions of D_{eff}, made using Eq. 5 which is a model for diffusion-adsorption in a porous medium. The parameters used are listed in Table 2. The adsorption constant K_{ads} was obtained from adsorption isotherms (Figure 4). The dimensionless adsorption constant R was calculated using Eq. 11. The void fraction is $\varepsilon = 1 - \phi$, where ϕ is the fiber volume fraction. The volume fraction is calculated from the mass fraction X_m as[37]

$$\phi = \frac{X_m}{X_m + \rho_f/\rho_w(1 - X_m)}, \tag{15}$$

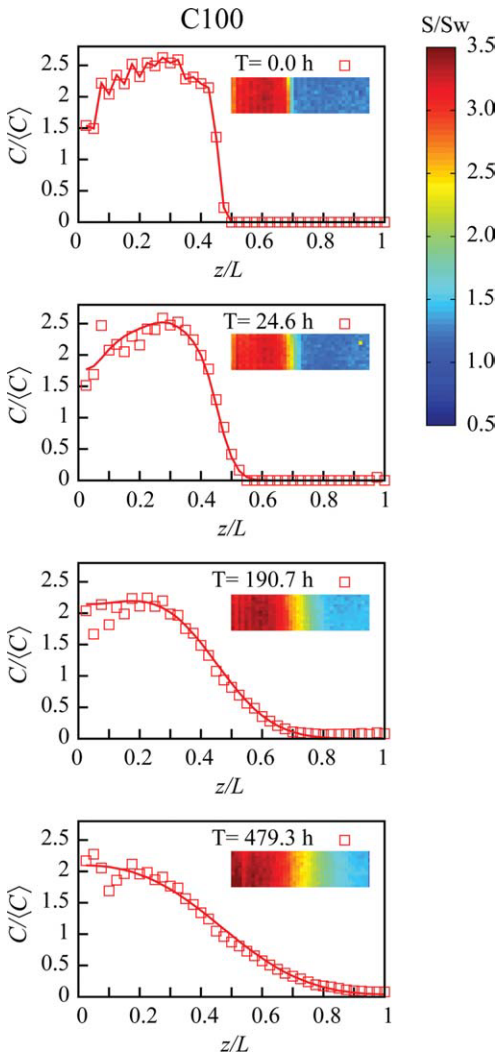

Figure 7. Normalized concentration profiles of $MnCl_2$ in C100 fibers.

Symbols are experimental values, lines are concentration profiles calculated using the numerical method. [Color figure can be viewed in the online issue, which is available at wileyonlinelibrary.com.]

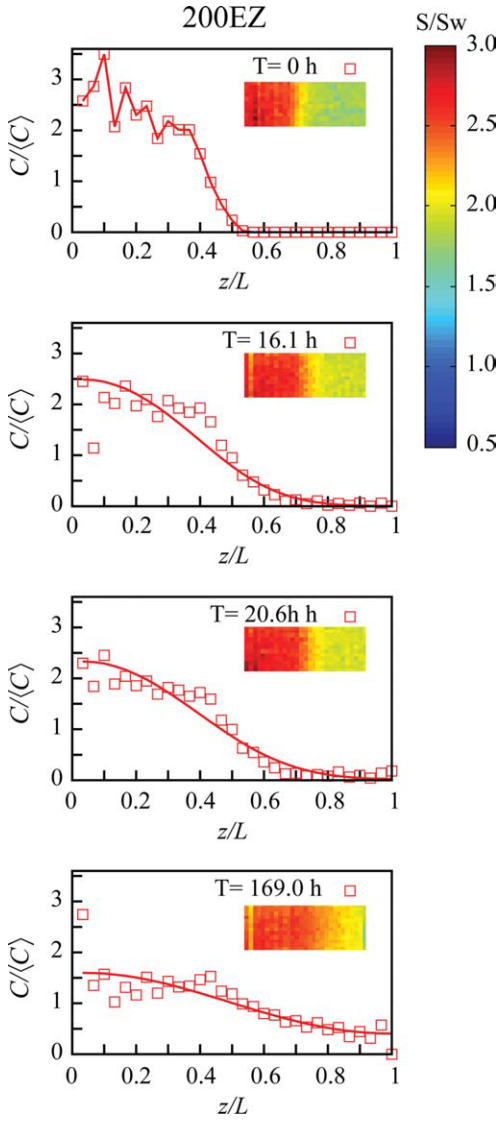

Figure 8. Normalized concentration profiles of $MnCl_2$ in 200EZ fibers.

Symbols are experimental values, lines are concentration profiles calculated using the numerical method. [Color figure can be viewed in the online issue, which is available at wileyonlinelibrary.com.]

where X_m is the unit mass fraction, $\rho_f = 1500$ kg/m^3 is the density of the cellulose fibers, and $\rho_w = 1000$ kg/m^3 is the density of water.

Since the exact geometry of the fiber bed is not known, we estimate τ based on porous media correlations that predict a tortuosity factor as a function of the void fraction ε. As $\varepsilon \rightarrow 1$, the tortuosity factor approaches unity. The relation between tortuosity and porosity at $\varepsilon > 0.7$ is very similar for various geometries.[38–41] Tortuosities calculated with various correlations are shown in Table 3 using void fractions ε of 0.91 and 0.88 for C100 and 200EZ fibers respectively. For estimating the diffusivity we consider two extreme cases: (a) The lowest tortuosity factors from Table 3 which are $\tau = 1.04$ for C100 and $\tau = 1.06$ for 200EZ.[38] (b) The highest tortuosity factors from Table 3 which are $\tau = 1.10$ for C100 and $\tau = 1.14$ for 200EZ.[39] Case (a) has been adopted in models of biomass pretreatment by Hosseini and Shah.[11,44]

As shown in Table 2 and Figure 9 the effective diffusivities predicted using Eq. 5 compare well with the experimental values. It must be emphasized that no adjustable parameters were used to obtain the predicted diffusivities of Figure 9. As mentioned above, in all cases the effective diffusivities in fiber beds are much lower than the bulk diffusivity. The presence of the fibers, therefore, presents a significant obstacle for diffusion of the solute.

Since void fractions and tortuosities are similar for both fiber types, the difference in effective diffusivities of the two fiber types is attributed to the large difference in the adsorption equilibrium constants as shown in Table 2. In light of the diffusion-adsorption model described above, the fiber concentration has a quadruple effect on the effective diffusivity. First, an increase in fiber loading causes a decrease in void fraction, to which the effective diffusivity is directly proportional. Such a linear decrease in diffusivity with fiber concentration was reported by Wong and Reeve[16] for diffusion of potassium chloride in various types of fiber suspensions. Second, an increase in fiber concentration causes an increase in the tortuosity factor, due to the reduced void fraction, as illustrated by the correlations in Table 3. Since the effective diffusivity is inversely proportional to the tortuosity factor, Eq. 5, this effect is compounded with the increase in void fraction causing a further reduction in the effective diffusivity as fiber concentration is increased. In contrast with the void fraction, which varies linearly with fiber concentration, the variation of tortuosity with concentration or void fraction is nonlinear. The effect of fiber concentration on tortuosity will be small at high void fractions $\varepsilon \rightarrow 1$, where $\tau \rightarrow 1$, but will be significant at lower void fractions, in a nonlinear fashion as given in Table 3. Table 3 also shows that the influence of particle geometry on tortuosity is more significant at high fiber concentrations than at low fiber

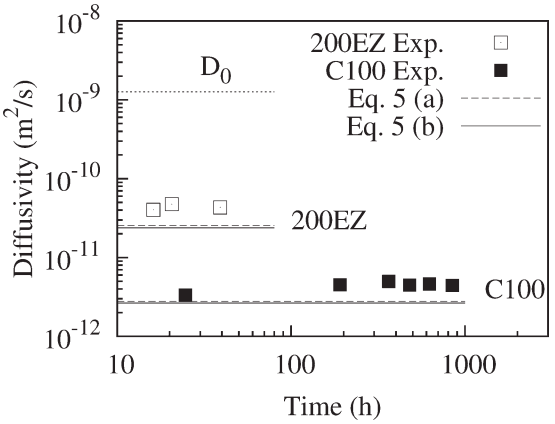

Figure 9. Diffusivity of $MnCl_2$. The top line is the bulk diffusivity $MnCl_2$.[17,36,33]

Experimental effective diffusivities for the two types of fibers as a function of experimental time are plotted as symbols. Lines near the symbols are the values predicted using Eq. 5.

Table 2. Diffusion-Adsorption Parameters

Variable	Symbol	Units	Fiber Type	
			C100	200EZ
Adsorption constant	K_{ads}	m^3/kg	2.71×10^0	1.97×10^{-1}
Adsorption constant	R	–	3.94×10^2	3.98×10^1
Void fraction	ε	–	0.91	0.88
Tortuosity factor (a)	τ	–	1.04	1.06
Diffusivity prediction (a)	D_{eff}	m^2/s	2.79×10^{-12}	2.56×10^{-11}
Tortuosity factor (b)	τ	–	1.10	1.14
Diffusivity prediction (b)	D_{eff}	m^2/s	2.64×10^{-12}	2.38×10^{-11}
Diffusivity, measured	D_{eff}^{Exp}	m^2/s	$(4.39 \pm 0.5) \times 10^{-12}$	$(4.37 \pm 0.4) \times 10^{-11}$

concentrations. Next, the fiber concentration affects the total solute adsorption, Eq. 11, and therefore the diffusivity on the fibers. In this case, increased fiber concentration is associated with an increase in adsorption sites. A high concentration of fibers in relation to the solute concentration in the mobile phase, leads to a reduction of the effective diffusivity proportional to $1/(1 + R)$. At low fiber concentrations, however, the effect of adsorption may be small and even negligible. If the number of adsorption sites is low enough that saturation occurs on all fibers, and a very small fraction of solute is removed from solution, the concentration of solute in the mobile phase will not be strongly influenced by the concentration on the adsorbed phase, and adsorption properties will have a very weak effect on diffusion rates. Adsorption effects become more complex if multiple adsorbing components are present and this is not considered here. Lastly, as previously noted by Wong and Reeve,[16] the fiber/water system may include trapped air bubbles, which act as further obstacles for solute diffusion. These air bubbles are less likely to be mobilized and expelled by their buoyancy in a concentrated fiber suspension that has a high yield stress. The presence of this trapped air can be regarded as a cause of further reduction in void fraction, with a consequent reduction in effective diffusivity. All four of these effects are summarized in Table 4.

The dependence of diffusivity on adsorption characteristics has direct consequences for the time required to achieve homogenization by diffusion. The results presented here suggest the use of homogenization strategies that take advantage of changes of adsorption behavior with variables such as temperature, pH, or ionic strength. For example, an initial mixing step can be performed at a temperature at which the solute is weakly adsorbed, facilitating homogenization by diffusion. A concentrated suspension with reduced diffusivity requires more intense convective mixing for homogenization, and mixing requires increased energy at higher suspension viscosities.[45] In this context, strategies to reduce viscosity are desirable, such as reducing the particles aspect ratio by mechanical size reduction,[46] or using additives to reduce interparticle friction.[47] Additives such as carboxymethyl cellulose (CMC), or a mixture of CMC and hydroxypropylmethylcellulose (HPMC) have been shown to be effective rheology modifiers for extrusion of fiber suspensions at ultra-high consistency (20–40% solids).[48]

Table 3. Tortuosity Correlations

Correlation	Remark	τ for Fiber Type		Ref.
		C100	200EZ	
$\tau = (3 - \varepsilon)/2$	Random sphere packing	1.04	1.06	[42]
$\tau = (2 - \varepsilon)$	Constricted pores	1.08	1.11	[43]
$\tau = (1 - 0.5\ln\varepsilon)$	Overlapping spheres	1.04	1.06	[38]
$\tau = ((1 - 0.33)/(\varepsilon - 0.33))^{0.707}$	Fibers 1D perpendicular	1.10	1.14	[39]
$\tau = ((1 - 0.11)/(\varepsilon - 0.11))^{0.521}$	Fibers 2D parallel	1.05	1.07	[39]
$\tau = ((1 - 0.11)/(\varepsilon - 0.11))^{0.785}$	Fibers 2D perpendicular	1.08	1.11	[39]
$\tau = ((1 - 0.037)/(\varepsilon - 0.037))^{0.661}$	Fibers 3D random	1.06	1.09	[39]

Conclusions

The effective diffusivity of an adsorbing solute in mixtures of cellulosic fibers and water was calculated from concentration profiles measured using MR imaging. The temporal evolution of the concentration profiles was compared with numerical simulations of one-dimensional Fickian diffusion using the initial measured concentration profile as the initial condition. The measured effective diffusivities were approximately constant in time, highly dependent on fiber type, and significantly lower than the bulk diffusivity of the solute. The two types of suspensions used in this study had small differences in their void fraction and tortuosity and differed the most in the adsorption equilibrium constants of their fibers. The measured effective diffusivities show that strong adsorption is associated with slow diffusion, in agreement with a diffusion-adsorption model for porous media.[30] According to the model, an increase in fiber concentration will cause a decrease in diffusion rates due to four effects: (a) Reduction in void fraction; (b) Increase in tortuosity; (c) Increased number of adsorption sites per mol of solute; (d) Increased tendency to trap air. A possible mixing strategy based on the present results would be to use

Table 4. Effect of Suspension Variables on Effective Diffusivity

Variable (Symbol)	Effect of Changes in ϕ	Effect on D_{eff}
Void faction (ε)	$\uparrow\phi \Rightarrow \downarrow\varepsilon$	$\downarrow\varepsilon \Rightarrow \downarrow D_{eff}$
Tortuosity (τ)	$\uparrow\phi \Rightarrow \uparrow\tau$	$\uparrow\tau \Rightarrow \downarrow D_{eff}$
Adsorption constant (R)	$\uparrow\phi \Rightarrow \uparrow R$	$\uparrow R \Rightarrow \downarrow D_{eff}$
Gas volume fraction (ϕ_g)	$\uparrow\phi \Rightarrow \uparrow\phi_g$	$\uparrow\phi_g \Rightarrow \downarrow D_{eff}$

conditions that favor high diffusion rates and facilitate homogenization, prior to bringing the system to optimal conditions for the reactions of interest. A goal for future studies is to measure and model diffusion in various cellulosic fiber types of solute molecules of large size, comparable with the enzymes used in the biomass hydrolysis process.

Acknowledgments

Fiber length measurements were provided by Tom Lindström from Innventia AB, Stockholm, Sweden. Aspect AI, Hevel Modi'in Industrial Area, Israel provided pulse sequences used in the study. Partial financial support provided by an award from the Center for Process Analytical Chemistry of the University of Washington, Seattle, WA.

Notation

C = solute concentration, per unit volume of suspension, mol/m^3
$C_{\mathrm{Exp}}(z)$ = experimental solute concentration at position z, per unit volume of suspension, mol/m^3
$C_{\mathrm{Num}}(z)$ = numerical solute concentration at position z, per unit volume of suspension, mol/m^3
$\langle C \rangle$ = spatially averaged solute concentration, per unit volume of suspension, mol/m^3
$\langle C_{\mathrm{Exp}} \rangle$ = spatially averaged experimental solute concentration, per unit volume of suspension, mol/m^3
$\langle C_{\mathrm{Num}} \rangle$ = spatially averaged numerical solute concentration, per unit volume of suspension, mol/m^3
C_{adsorbed} = concentration of solute in the solid phase, per unit volume of suspension, mol/m^3
C_{mobile} = concentration of solute in the mobile phase, per unit volume of suspension, mol/m^3
C_{mobile}' = concentration of solute in the mobile phase, per unit volume of liquid, mol/m^3
z = position, m
t = time, s
$\Delta\hat{t}$ = dimensionless time step used in the numerical method
$D_{\mathrm{eff}}^{\mathrm{Porous}}$ = effective diffusivity in a porous medium without adsorption, m^2/s
$D_{\mathrm{eff}}^{\mathrm{Adsorbing}}$ = effective diffusivity in an homogenous adsorbing medium, m^2/s
D_{eff} = effective diffusivity in a porous medium with adsorption, m^2/s
$D_{\mathrm{eff}}^{\mathrm{Exp}}$ = experimentally measured effective diffusivity, m^2/s
D_0 = bulk diffusivity, m^2/s
ε = void fraction, dimensionless
ϕ = volume fraction of fibers, dimensionless
X_{m} = mass fraction of fibers, dimensionless
ϕ_{g} = volume fraction of gas, dimensionless
τ = tortuosity factor, dimensionless
R = equilibrium constant of the linear adsorption equilibrium, dimensionless
K_{ads} = initial slope of adsorption isotherm, m^3/Kg
Γ^{∞} = parameter of Langmuir isotherm, mol/Kg
k = parameter of Langmuir isotherm, m^3/mol
m = mass of fibers, g
V = volume of liquid, m^3
V_{total} = volume of suspension, m^3
L = fiber bed length, m

Literature Cited

1. Um B, Hanley TR. High-solids enzymatic hydrolysis and fermentation of Solka-Floc into ethanol. *J Microbiol Biotechnol*. 2008;18:1257–1265.
2. Dasari RK, Dunaway K, Berson E. A scraped surface bioreactor for enzymatic saccharification of pretreated corn stover slurries. *Energy Fuels*. 2009;23:492–427.
3. Varga E, Klinke HB, Reczery K, Thomsen AB. High solid simultaneous saccharification and fermentation of wet oxidized corn stover to ethanol. *Biotechnol Bioeng*. 2004;88:567–574.
4. Galbe M, Sassner P, Wingren A, Zacchi G. Process engineering economics of bioethanol production. *Adv Biochem Eng/Biotechnol*. 2007;108:303–327.
5. Vane LM. Separation technologies for the recovery and dehydration of alcohols from fermentation broths. *Biofuels Bioprod Bioref*. 2008;2:553–588.
6. Sassner P, Galbe M, Zacchi G. Techno-economic evaluation of bioethanol production from three different lignocellulosic materials. *Biomass Bioenerg*. 2008;32:422–430.
7. Ariff AB, Asbi BA, Azudin MN, Kennedy JF. Effect of mixing on enzymatic liquefaction of sago starch. *Carbohyd Polym*. 1997;33:101–108.
8. Roche C, Dibble C, Stickel J. Laboratory-scale method for enzymatic saccharification of lignocellulosic biomass at high-solids loadings. *Biotechnol Biofuels*. 2009;2:28.
9. Jones SW. The enhancement of mixing by chaotic advection. *Phys Fluids A*. 1990;3:1081–1086.
10. Hardt S, Penneman H, Schonfeld F. Theoretical and experimental characterization of a low-Reynolds number split-and-recombine mixer. *Microfluid Nanofluid*. 2006;2:237–248.
11. Hosseini SA, Shah N. Multiscale modelling of biomass pretreatment for biofuels production. *Chem Eng Res Des*. 2009;87:1251–1260.
12. Burr HK, Stamm AJ. Diffusion in wood. *J Phys Chem*. 1947;51:240–261.
13. Viamajala S, Selig MJ, Vinzant TB, Tucker MP, Himmel ME, McMillan JD, Decker SR. Catalyst transport in corn stover internodes: elucidating transport mechanisms using Direct Blue-I. *Appl Biochem Biotech*. 2006;129–132:509–527.
14. Kim SB, Lee YY. Diffusion of Sulfuric acid within lignocellulosic biomass particles and its impact on dilute-acid pretreatment. *Bioresource Technol*. 2002;83:165–171.
15. Paterson AHJ, Kerekes RJ. Fundamentals of mixing in pulp suspensions: diffusion of reacting chlorine. *TAPPI J*. 1984;67:114–117.
16. Wong BM, Reeve DW. Diffusion in fibre beds. *J Pulp Pap Sci*. 1990;16:J72–J76.
17. Cussler EL. *Diffusion: Mass Transfer in Fluid Systems*. 2nd ed. New York: Cambridge University Press, 1997.
18. Epstein N. On tortuosity and the tortuosity factor in flow and diffusion through porous media. *Chem Eng Sci*. 1989;44:777–779.
19. Kumar R, Wyman CE. Cellulase adsorption and relationship to features of corn stover solids produced by leading pretreatments. *Biotechnol Bioeng*. 2009;103:252–267.
20. Eriksson T, Borjesson J, Tjerneld F. Mechanism of surfactant effect in enzymatic hydrolysis of lignocellulose. *Enzyme Microb Tech*. 2002;31:353–364.
21. Alkasrawi M, Eriksson T, Borjesson J, Wingern A, Galbe M, Tjerneld F, Zacchi G. The effect of Tween-20 on simultaneous saccharification and fermentation of softwood to ethanol. *Enzyme Microb Tech*. 2003;33:71–78.
22. Kristensen JB, Borjesson J, Bruun MH, Tjerneld F, Jorgensen H. Use of surface active additives in enzymatic hydrolysis of wheat straw lignocellulose. *Enzyme Microb Tech*. 2007;40:888–895.
23. Zheng Y, Pan Z, Zhang R, Wang D, Jenkins B. Non-ionic surfactants and non-catalytic protein treatment on enzymatic hydrolysis of pretreated creeping wild ryegrass. *Appl Biochem Biotechnol*. 2008;146:231–248.
24. Xu F, Ding H, Osborn D, Tejirian A, Brown K, Albano W, Sheehy N, Langston J. Partition of enzymes between the solvent and insoluble substrate during the hydrolysis of lignocellulose by cellulases. *J Mol Catal B-Enzym*. 2008;51:42–48.
25. Bryant P, Petersen J, Lee J, Brouns T. Sorption of heavy metals by untreated red fir sawdust. *Appl Biochem Biotechnol*. 1992;34–35:777–788.
26. Bryant PS, Edwards LL. Manganese removal in closed kraft mill bleach plants. *TAPPI J*. 1994;77:137–148.
27. Kongdee A, Bechtold T. Influence of ligand type and solution ph on heavy metal ion complexation in cellulosic fibre: model calculations and experimental results. *Cellulose*. 2009;16:53–63.
28. Osaki S, Inoue E, Sugihara S, Takashima Y. Direct measurement of diffusion coefficients of Sr and Co in silica gel layers under various conditions. *J Radioanal Nucl Ch*. 1993;170:381–387.
29. Crank J. *The Mathematics of Diffusion*, 2nd ed. New York: Oxford University Press, 2002.

30. Weisz PB. Sorption-diffusion in heterogeneous systems. Part 1—general sorption behaviour and criteria. *T Faraday Soc*. 1967;63:1801–1806.
31. Deen WM. Hindered transport of large molecules in liquid-filled pores. *AIChE J*. 1987;33:1409–1425.
32. Phillips RJ, Deen WM, Brady JF. Hindered transport of spherical macro-molecules in fibrous membranes and gels. *AIChE J*. 1989;35:1761–1769.
33. Olson MS, Ford RM, Smith JA, Fernandez EJ. Analysis of column tortuosity for $MnCl_2$ and bacterial diffusion using magnetic resonance imaging. *Environ Sci Technol*. 2005;39:149–154.
34. Pulkkinen I, Ala-Kaila K, Aittamaa J. Characterization of wood fibers using fiber property distributions. *Chem Eng Process*. 2006;45:546–554.
35. Lee SB, Shin HS, Ryu DDY, Mandels M. Adsorption of cellulase on cellulose: effect of physicochemical properties of cellulose on adsorption and rate of hydrolysis. *Biotech Bioeng*. 1982;24:2137–2153.
36. Marder L, Ortega Navarro E, Perez-Herranz V, Bernardes A, Zopas Ferreira J. Evaluation of transition metals transport properties through a cation-exchange membrane by chronopotentiometry. *J Membrane Sci*. 2006;284:267–275.
37. Roche CM, Dibble CJ, Knutsen JS, Stickel JJ, Liberatore MW. Particle concentration and yield stress of biomass slurries during enzymatic hydrolysis at high-solids loadings. *Biotechnol Bioeng*. 2009;104:290–300.
38. Weissberg HL. Effective diffusion coefficient in porous media. *J Appl Phys*. 1963;34:2636–2639.
39. Tomadakis MM, Sotirchos SV. Ordinary and transition regime diffusion in random fiber structures. *AIChE J*. 1993;39:397–412.
40. Tomadakis MM, Sotirchos SV. Transport properties of random arrays of freely overlapping cylinders with various orientation distributions. *J Chem Phys*. 1993;98:616–626.
41. Shen L, Chen Z. Critical review of the impact of tortuosity on diffusion. *Chem Eng Sci*. 2007;62:3748–3755.
42. Neale GH, Nader WK. Prediction of transport processes within porous media: diffusive flow processes within an homogeneous swarm of spherical particles. *AIChE J*. 1973;19:112–119.
43. Petersen EE. Diffusion in a pore of varying cross section. *AIChE J*. 1958;4:343–345.
44. Hosseini SA, Shah N. Multiscale modelling of hydrothermal biomass pretreatment for chip size optimization. *Bioresource Technol*. 2009;100:2621–2628.
45. Zhang J, Chu D, Huang J, Yu Z, Dai G, Bao J. Simultaneous saccharification and ethanol fermentation at high corn stover solids loading in a helical stirring bioreactor. *Biotechnol Bioeng*. 2010;105:718–728.
46. Hennessey S, Seapan M, Elander RT, Tucker M. Process for concentrated biomass saccharification. United States Patent Application No. 20090053777, 2009.
47. Knutsen JS, Liberatore MW. Rheology modification and enzyme kinetics of high solids cellulosic slurries. *Energ Fuel*. 2010;24:3267–3274.
48. Scott CT. Pulp Extrusion at ultra-high consistencies: selection of water soluble polymers for process optimization. Proceedings of the 2002 TAPPI Fall Technical Conference and Trade Fair. San Diego, CA. Atlanta, GA: TAPPI Press, 2002: 105–114.

Manuscript received Aug. 16, 2010, and revision received Jan. 5, 2011.